Simultaneous Imaging of Amyloid-β and Lipids in Brain Tissue Using Antibody-Coupled Liposomes and Time-of-Flight Secondary Ion Mass Spectrometry

ARTICLE *in* JOURNAL OF THE AMERICAN CHEMICAL SOCIETY · JUNE 2014

Impact Factor: 12.11 · DOI: 10.1021/ja5019145 · Source: PubMed

11 AUTHORS, INCLUDING:

Anders Gunnarsson
Chalmers University of Technology
23 PUBLICATIONS **245** CITATIONS
SEE PROFILE

Alina Codita
Karolinska Institutet
20 PUBLICATIONS **176** CITATIONS
SEE PROFILE

Martin Schalling
Karolinska Institutet
325 PUBLICATIONS **15,474** CITATIONS
SEE PROFILE

Fredrik Höök
Chalmers University of Technology
149 PUBLICATIONS **7,519** CITATIONS
SEE PROFILE

JACS
JOURNAL OF THE AMERICAN CHEMICAL SOCIETY
Article
pubs.acs.org/JACS

Simultaneous Imaging of Amyloid-β and Lipids in Brain Tissue Using Antibody-Coupled Liposomes and Time-of-Flight Secondary Ion Mass Spectrometry

Louise Carlred,[†,‡] Anders Gunnarsson,[‡,#] Santiago Solé-Domènech,[§,▽] Björn Johansson,[§] Vladana Vukojević,[∥] Lars Terenius,[∥] Alina Codita,[⊥] Bengt Winblad,[⊥] Martin Schalling,[§] Fredrik Höök,[‡] and Peter Sjövall*[,†,‡]

[†]Chemistry, Materials and Surfaces, SP Technical Research Institute of Sweden, P.O. Box 857, SE-501 15 Borås, Sweden
[‡]Department of Applied Physics, Division of Biological Physics, Chalmers University of Technology, SE-412 96 Göteborg, Sweden
[§]Department of Molecular Medicine and Surgery, Karolinska Institutet, SE-171 76 Stockholm, Sweden
[∥]Department of Clinical Neuroscience, Karolinska Institutet, SE-171 76 Stockholm, Sweden
[⊥]Department of Neurobiology, Care Sciences and Society, KI Alzheimer Disease Research Center, Karolinska Institutet, SE-141 86 Stockholm, Sweden

Supporting Information

ABSTRACT: The spatial localization of amyloid-β peptide deposits, the major component of senile plaques in Alzheimer's disease (AD), was mapped in transgenic AD mouse brains using time-of-flight secondary ion mass spectrometry (ToF-SIMS), simultaneously with several endogenous molecules that cannot be mapped using conventional immunohistochemistry imaging, including phospholipids, cholesterol and sulfatides. Whereas the endogenous lipids were detected directly, the amyloid-β deposits, which cannot be detected as intact entities with ToF-SIMS because of extensive ion-induced fragmentation, were identified by specific binding of deuterated liposomes to antibodies directed against amyloid-β. Comparative investigation of the amyloid-β deposits using conventional immunohistochemistry and fluorescence microscopy suggests similar sensitivity but a more surface-confined identification due to the shallow penetration depth of the ToF-SIMS signal. The recorded ToF-SIMS images thus display the localization of lipids and amyloid-β in a narrow (~10 nm) two-dimensional plane at the tissue surface. As compared to a frozen nontreated tissue sample, the liposome preparation protocol generally increased the signal intensity of endogenous lipids, likely caused by matrix effects associated with the removal of salts, but no severe effects on the tissue integrity and the spatial distribution of lipids were observed with ToF-SIMS or scanning electron microscopy (SEM). This method may provide an important extension to conventional tissue imaging techniques to investigate the complex interplay of different kinds of molecules in neurodegenerative diseases, in the same specimen. However, limitations in target accessibility of the liposomes as well as unspecific binding need further consideration.

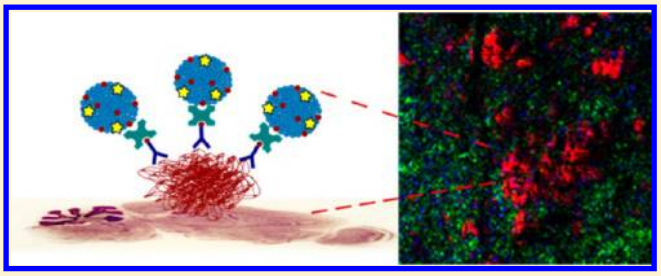

INTRODUCTION

Lipids are major components of mammalian cell membranes and are currently gaining increased recognition as important functional components in many cellular processes such as cell growth, migration and death,[1] typically in close interplay with proteins and metabolites. In particular, the critical role of lipids in a variety of medical disorders, including neurodegenerative diseases such as Alzheimer's disease (AD),[2] is currently being revealed as advanced techniques to study lipids, in particular mass spectrometry, are developed. Although the role of lipids in AD is not completely understood, recent studies[2−4] have found that deregulation of lipid function is involved in the amyloidogenic process, i.e., the formation of so-called senile plaques consisting of amyloid-β peptides, which is one of the characteristic features of AD.[5] One of the lipid molecules that affects the pathogenic process in AD is cholesterol,[4] which is likely linked to the disease via apolipoprotein E (APOE), the main cholesterol transporter within the central nervous system. In fact, the E4 allele variant of the APOE gene is currently known as the major genetic risk factor to develop AD.[5] Furthermore, increased levels of cholesterol correlate with increased production of amyloid-β peptides in lipid rafts and aggregation of amyloid-β into toxic fibrils and deposits.[6,7] In addition, it is known that sulfatide levels are dramatically reduced in patients with mild cognitive impairment (MCI), a condition that may later progress to Alzheimer's disease, while ceramide levels are significantly increased in these patients.[8]

Received: February 24, 2014
Published: June 18, 2014

dx.doi.org/10.1021/ja5019145 | J. Am. Chem. Soc. 2014, 136, 9973−9981

The possibility to localize and quantitatively characterize the amount of cholesterol, sulfatides, and other lipids in relation to amyloid-β is thus of high relevance as it might shed light into AD pathogenesis, but remains still a challenge.

In this work, we demonstrate a new method to use imaging mass spectrometry (IMS) to simultaneously map the distribution of amyloid-β peptides and several endogenous lipids in brain tissue. IMS is an emerging analytical technology for analysis of biomolecules in tissue samples with the potential to provide a powerful alternative to traditional tissue imaging techniques, such as immunohistochemistry. An important advantage of IMS is the capability to image the spatial distribution of many different biomolecules in parallel without the need for preselection or labeling. In contrast, immunohistochemical approaches provide unrivaled sensitivity and spatial resolution by utilizing binding of antibodies to specific molecules of interest; however, the mode of detection, e.g., confocal fluorescence microscopy, typically allows for the analysis of only 3−4 different analytes in parallel. Furthermore, most antibodies only recognize different kinds of proteins, while other molecules, such as specific lipids, cannot be detected with this method. Since there is an increasing interest in analyzing both lipids and proteins in tissue samples, IMS has emerged as a potential alternative to traditional tissue imaging, allowing for parallel detection of many different biomolecules.[9,10]

Matrix-assisted laser desorption/ionization (MALDI) mass spectroscopy is an IMS technique suitable for detection of peptides and proteins, as well as lipids in biological tissue samples.[11,12] The major drawback with this technique is the spatial resolution, which typically is limited by the spot size of the laser beam to ∼50 μm.[11] Also, the use of a matrix on top of the sample is a complicating factor that needs to be optimized for particular analytes and samples studied and, in addition, may interfere with detection of molecules with a molecular weight in the same range as the matrix. On the other hand, the matrix also increases the ionization probability of molecules at the surface, resulting in higher sensitivities in comparison to other mass spectrometry techniques.

Time-of-flight secondary ion mass spectrometry (ToF-SIMS) is another IMS method that can be used for detection and localization of a wide range of low molecular weight analytes (<1−2 kDa) in biological tissue samples, at spatial resolutions down to the submicrometer range.[10] ToF-SIMS is especially suitable for the analysis of lipids, generating novel insights about the distribution of, e.g., phospholipids, cholesterol, sulfatides, galactosylceramide and vitamin E in mouse and rat brain tissue.[11,13−15] ToF-SIMS has also been used to investigate changes in lipid distributions in connection to different diseases, such as the degenerative genetic disease Duchenne muscular dystrophy (DMD)[16] and Alzheimer's disease (AD).[17,18]

In contrast to lipids, most peptides and proteins are too large to be identified with ToF-SIMS in complex samples, since fragmentation by the primary ion beam (during the sputtering process) prevents their detection as intact molecules. However, since ToF-SIMS analysis only affects the topmost surface (<20 nm),[19] proteins of interest can be subsequently imaged in the same tissue section using complementary techniques such as MALDI[11] or immunohistochemistry.[17] One difficulty with this approach is to localize the same area of analysis with the different methods and there is also a potential risk to disturb the tissue integrity in-between the different analyses.[20] Furthermore, limitations of the complementary techniques will remain, i.e., the limited spatial resolution of MALDI and the limited number of proteins that can be analyzed in parallel by immunohistochemistry.

Another powerful IMS technique is dynamic secondary ion mass spectrometry (SIMS), which can detect elements and small fragments with a spatial resolution down to ∼50 nm.[21,22] Recently, Wilson et al. reported simultaneous detection of lipids and proteins in cells using the NanoSIMS instrument with fluorinated colloidal gold immunolabels for protein detection.[23] However, since dynamic SIMS, e.g., using the NanoSIMS instrument, only detects small (mainly monoatomic and diatomic) ions, simultaneous lipid imaging is limited to lipids carrying stable isotopes,[24] thus preventing the feasibility of this approach to investigate unknown endogenous lipids.

The approach developed here for simultaneous imaging of lipids and proteins utilizes ToF-SIMS, and is based on a combination of conventional mapping of the lipid distribution in the tissue sample[13−15] with specific protein detection using biotinylated lipid vesicles, here called liposomes, which were linked to the protein of interest using biotinylated antibodies and neutravidin. In this way, the liposomes act as a signal enhancer, with each liposome (containing ∼200 000 lipids) in principle correlating to one single protein on the tissue surface.[25] The liposomes were distinguished from the endogenous lipids in the tissue by using deuterated lipids in the liposomes, thus enabling simultaneous mapping of proteins and lipids with submicrometer spatial resolution. Specific binding of antibody-coupled liposomes to amyloid-β was confirmed through complementary analysis by fluorescence microscopy, including a small percentage of fluorescently labeled lipids in the liposomes, and by traditional immunohistochemistry analysis of adjacent tissue sections. Furthermore, any effects the tissue preparation protocol may have on lipid composition and distribution were carefully monitored, as several tissue sample preparation protocols have been shown to modify the surface distribution of analytes as well as tissue integrity.[20,26−28] The capability of the method was demonstrated by imaging of amyloid-β and its spatial localization in comparison with a number of endogenous lipids, including cholesterol, sulfatides and phosphatidylcholine, in brain tissue from a transgenic mouse model of AD.

EXPERIMENTAL SECTION

Preparation of Tissue Sections from Mouse Brains. Mouse brains were obtained from 22 months old transgenic female mice of the Tg2576 model of AD, expressing the human APP695 isoform of the Swedish double mutation K670N-M671L[29] (Taconic, Cologne, Germany). The mice were killed by cervical dislocation and the brains were quickly dissected and frozen on dry ice, followed by storage at −80 °C. Sagittal sections of 16 μm thickness were cut using a cryostat (Leica Jung CM 3000, Leica Microsystems, Germany) at approximately −20 °C. Sections were collected on Superfrost Plus glass slides (Gerhard Menzel GmbH, Germany) and stored in a freezer at −20 °C until analysis. Sections cut at 2.88−2.90 mm from the brain's midline were selected for analysis.

Preparation of Liposomes. Small unilamellar liposomes containing 98 wt % deuterated POPC, 1-palmitoyl-2-oleoyl-*sn*-glycero-3-phosphocholine-1,1,2,2-d4-*N*,*N*,*N*-trimethyl-d9 (D13-POPC, customized order from Avanti Polar Lipids, Inc., USA), 1 wt % 1,2-dioleoyl-*sn*-glycero-3-phosphoethanolamine-*N*-(biotinyl) (DOPE-biotin, Avanti Polar Lipids) and 1 wt % lissamine rhodamine B 1,2-dihexadecanoyl-*sn*-glycero-3-phosphoethanolamine (DHPE-Rhodamine, Invitrogen, Life Technologies, USA) were prepared by mixing 2 mg of lipids dissolved in chloroform/methanol, followed by

dx.doi.org/10.1021/ja5019145 | J. Am. Chem. Soc. 2014, 136, 9973−9981

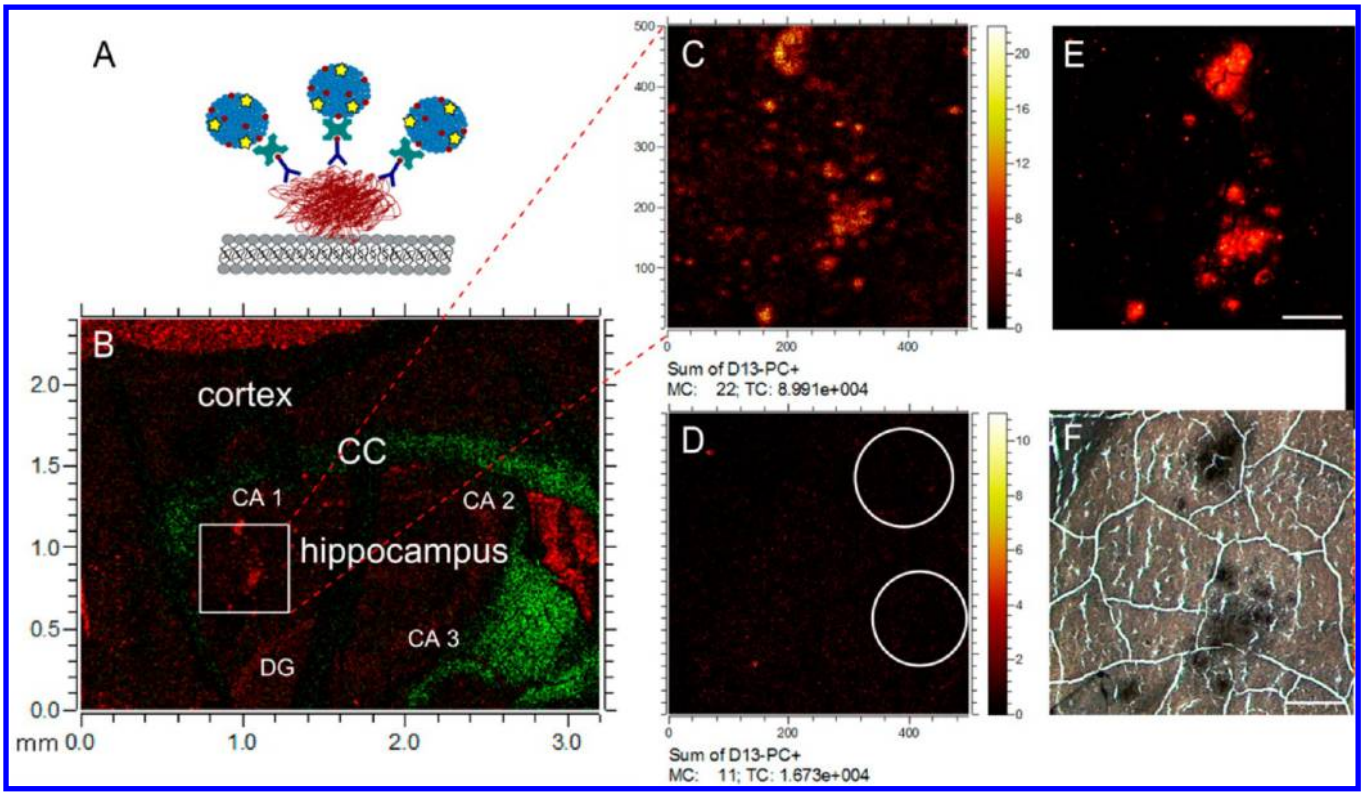

Figure 1. (A) Schematic illustration of the protein detection principle showing the binding of biotinylated liposomes, neutravidin and biotinylated antibodies (6E10) to an amyloid-β deposit in a tissue section. (B) ToF-SIMS overview image visualizing liposomes (red) and cholesterol (green) in the hippocampal region of a transgenic AD mouse brain section. CC and DG refer to corpus callosum and dentate gyrus regions, respectively. CA1, CA2 and CA3 refer to different areas of the Cornu Ammonis. Red areas above the cortex and to the right of the hippocampus indicate unspecific binding of liposomes to areas where the glass microscope slide is exposed. (C,D) ToF-SIMS images of the area indicated by the white square in (B) visualizing (C) amyloid-β deposits stained by antibody-coupled liposomes and (D) corresponding area in an adjacent tissue section incubated without the addition of antibodies (6E10). The position of amyloid-β deposits is indicated by the white circles. (E) Fluorescence microscopy image (10× magnification) of the same area analyzed by ToF-SIMS in (C), visualizing amyloid-β deposits stained by fluorescent lipids incorporated in the antibody-coupled liposomes. (F) Optical (bright field) microscopy image (10× magnification) of the same tissue sample as in (C) and (E). Scale bar = 100 μm.

drying in a round-bottom flask, first in a flow of nitrogen and then in a vacuum for 1 h to evaporate all organic solvent. The dried thin film of lipids was rehydrated in 1 mL of phosphate buffered saline (PBS, 0.01M, pH 7.6, Sigma-Aldrich) by vortexing for 5 min and the resulting solution was extruded through a 400 nm polycarbonate membrane filter 11 times to form small unilamellar liposomes. The final suspension of liposomes (2 mg/mL) was stored in a refrigerator at 4 °C. The liposome diameter determined with nanoparticle tracking analysis (NTA) (Nanosight Limited, UK) was 215 ± 70 nm, in agreement with liposome size determinations using other techniques.[30,31]

Immunohistochemistry and Confocal Laser Scanning Microscopy (CLSM). Mouse brain sections were stained for amyloid-β deposits using the monoclonal primary antibody 6E10 (Covance Research Products Inc., USA), reactive to the 1−16 amino acid residues of the amyloid-β peptide, in combination with liposomes or (for reference) a fluorescent secondary antibody (Alexa Fluor 555 goat antimouse, Invitrogen, Life Technologies). The tissue samples were first thawed and dried at room temperature for 1 h, followed by fixation with 4% paraformaldehyde (PFA, Sigma-Aldrich, USA) for 10 min. The tissue was then rinsed in PBS (0.01 M, pH 7.4, Medicago, Sweden) and incubated with blocking solution containing 5% normal goat serum (NGS, Invitrogen, Life Technologies), 2% bovine serum albumin (BSA, Sigma-Aldrich) and 0.3% Triton-X100 (Sigma-Aldrich) for 1 h. For liposome staining, the tissue was then incubated with biotinylated 6E10 (1 mg/mL diluted 1:1000 in a diluent solution containing 1% NGS, 0.01% BSA and 0.3% Triton-X100) overnight at 4 °C. Next, the tissue sample was incubated with 10 μg/mL neutravidin (Invitrogen, Life Technologies) for 1 h, followed by incubation with liposomes (0.1 mg/mL) for 24 h at 4 °C. Each incubation step was followed by thorough rinsing in PBS. A control sample was prepared by incubating the fixed tissue with the diluent solution (same as above) without 6E10 and excluding neutravidin incubation prior to liposomes in order to estimate the extent of unspecific binding of the liposomes.

For staining with secondary antibodies, an additional tissue sample was fixed with PFA and incubated with 6E10 (nonbiotinylated) as described above, followed by incubation with Alexa Fluor 555 goat antimouse (2 mg/mL diluted 1:800 in the diluent solution described above) for 1 h at room temperature. Also here a control sample was prepared by incubating the fixed tissue with the diluent solution without 6E10 in order to estimate unspecific binding of the secondary antibodies.

For analysis by confocal fluorescence microscopy, the stained tissue samples were rinsed and mounted with DAKO fluorescence aqueous mounting media (DAKO Denmark A/S), dried for 2 h at room temperature and imaged using confocal laser scanning microscopy (CLSM, ConfoCor3 system, Carl Zeiss, Germany). Fluorescence was excited using the HeNe543 laser, excitation wavelength of 543 nm. Emitted fluorescence was collected using a long pass filter at 580 nm. Recorded images were processed using the open source software ImageJ (http://rsb.info.nih.gov/ij/).

ToF-SIMS Analysis. Imaging ToF-SIMS analyses of the tissue samples were conducted in the static SIMS regime, which means that the results are obtained mainly from sample areas that have not been subjected to primary ion bombardment. The static SIMS conditions are important in order to obtain molecular information at high spatial

dx.doi.org/10.1021/ja5019145 | J. Am. Chem. Soc. 2014, 136, 9973−9981

resolutions, since the primary ions used in this work, generated in a liquid metal ion gun to achieve high spatial resolution, produce extensive molecular damage at the ion impact area on the sample surface. Static SIMS thus only probes the outermost molecular layers of the sample surface. A sampling depth of <10 nm was previously verified in our instrument by depth profile measurements of an organic multilayered reference sample, which showed a depth resolution of 10 nm using the same analysis parameters as in this study.[32]

For ToF-SIMS analysis, tissue samples were fixed with PFA and incubated with biotinylated 6E10, neutravidin and liposomes as described above, with the addition of an extra blocking step using ordinary POPC-liposomes labeled with 1% NBD-PE (*N*-(7-nitrobenz-2-oxa-1,3-diazol-4-yl)-1,2-dihexadecanoyl-*sn*-glycero-3-phosphoethanolamine, Invitrogen, Life Technologies) (0.1 mg/mL) for 1 h. After addition of the D13-POPC liposomes the tissue sample was rinsed with PBS and the volatile salt buffer ammonium formate (AF, 150 mM, pH 7.4 Sigma-Aldrich). The tissue samples were then plunge-frozen in liquid propane at −185 °C (EMS 0002, Electron Microscopy Sciences, Inc., USA) and freeze-dried on a cold surface overnight in a vacuum chamber. Prior to ToF-SIMS analysis, the freeze-dried tissue samples were analyzed in a fluorescence microscope (Olympus BX 63, Japan) using an ET-Cy3 filter cube (Chroma Technology Corporation, USA) for Rhodamine fluorescence.

The tissue samples were analyzed with a ToF-SIMS IV instrument (ION-TOF GmbH, Germany) using 25 keV Bi_3^+ primary ions and low-energy electron flooding for charge-compensation. Data was acquired with the instrument optimized for high mass resolution (bunched mode, mass resolution $m/\Delta m \approx 5000$, lateral resolution ≈ 3−5 μm) with a pulsed current of 0.10 pA, or for high image resolution (burst alignment mode, mass resolution $m/\Delta m \approx 300$, lateral resolution ≈ 400 nm), with a current of 0.04 pA. The accumulated primary ion dose density (PIDD) was always kept below 1×10^{12} cm^{-2}, in order to ensure static SIMS conditions. By rastering the ion beam over the tissue sample, images were acquired of both positive and negative ions. Initially, an overview image of 3.2 × 2.4 mm^2 was acquired in bunched mode, using stage-scan with 200 pixels/mm and 5 shots/pixel, to localize suitable regions for further analysis. Images of 500 × 500 μm^2 were then acquired in bunched mode with 256 × 256 pixels, and finally, high resolution images of 200 × 200 μm^2 were recorded in burst alignment mode with 512 × 512 pixels. Analyzed mass peaks are shown in Table S1 in Supporting Information. Recorded positive and negative ion images were aligned with Adobe Photoshop Elements 9 (Adobe Systems Inc., USA) and processed further with ImageJ to produce overlay images.

Some tissue samples were analyzed frozen, prior to fixation and liposome incubation, in order to investigate possible effects of the liposome incubation procedure on the lipid distribution on the tissue surface. For these measurements, the frozen sample was mounted on the sample holder submerged in liquid nitrogen, followed by immediate insertion into the ToF-SIMS chamber. The analysis of these samples were performed with the same settings as above but with the sample temperature fixed at −80 °C. After ToF-SIMS analysis at −80 °C, the tissue samples were thawed, fixed with PFA and incubated with liposomes as described above and again analyzed (at room temperature) in the same analysis areas.

Scanning Electron Microscopy (SEM) Analysis. Some tissue samples were imaged with SEM (Zeiss Supra 40VP FEG, Germany) after ToF-SIMS analysis, in order to monitor possible changes in tissue surface morphology caused by the different preparation steps. Analysis was performed on uncoated tissue samples using an Everhardt−Thornley secondary electron detector at 0.8 keV electron energy. Two different analysis schemes were applied to investigate the effect of rinsing and plunge freezing, with or without prior PFA fixation, on the structure of the freeze-dried tissue surface. In the first measurement, an untreated tissue sample was freeze-dried in a vacuum and analyzed with ToF-SIMS followed by SEM. Then, the same tissue sample was rinsed in AF, plunge-frozen in liquid propane at −185 °C and freeze-dried overnight in a vacuum, and reanalyzed with SEM. In the second measurement, the tissue sample was fixed with PFA before rinsing in AF, followed by plunge-freezing and freeze-drying as above and, finally, analysis with SEM. In order to analyze the same region of the mouse brain after each preparation step, an easily recognizable region, arbor vitae in cerebellum, was chosen. The recorded SEM images were aligned with the corresponding ToF-SIMS images of the same analysis area using Adobe Photoshop Elements 9.

RESULTS AND DISCUSSION

ToF-SIMS Detection of Antibody-Coupled Liposomes. The approach using antibody-coupled liposomes for detection and localization of amyloid-β with ToF-SIMS is schematically illustrated in Figure 1A. Liposomes made of deuterated lipids (in order to be distinguished from endogenous lipids in the tissue) and biotinylated lipids were immobilized to the protein of interest (amyloid-β) on the tissue surface using biotinylated antibodies (6E10) and neutravidin. Neutravidin, which is a protein with four different binding sites for biotin, is acting as a linker by binding to both the biotinylated antibodies and the biotinylated lipids in the liposome. Detection of the immobilized liposomes during subsequent ToF-SIMS analysis then corresponds to the detection of amyloid-β, allowing for simultaneous analysis of amyloid-β deposits and endogenous lipids on the same tissue surface area.

Representative results of a ToF-SIMS analysis based on this approach, using deuterated liposomes (D13-POPC) to localize amyloid-β deposits in a transgenic AD mouse brain, are shown in Figure 1. In the overview ion image (Figure 1B) several spots with strong signal from D13-POPC (red) are visible, particularly in the hippocampus region. The hippocampus, which is known to be one of the most affected brain regions in Alzheimer's disease,[5] is located ventrally (below) to the distinct white matter border (corpus callosum, CC) identified in the ToF-SIMS ion image by the high cholesterol signal (green, Figure 1B). Analysis of a specific region with abundant D13-POPC signal (Figure 1C) reveals a number of structures resembling amyloid-β deposits, in both size and shape.[17] Furthermore, amyloid-β deposits can be observed in the optical (bright field) microscopy image from the same area as dark features in the tissue section (Figure 1F), and comparison with the D13-POPC image in ToF-SIMS demonstrates a close match in the pattern of spots, providing compelling evidence that the D13-POPC signal in ToF-SIMS indeed corresponds to amyloid-β deposits.

Using the incorporated fluorescently labeled lipids in the liposomes, the antibody-coupled liposomes could also be detected with fluorescence microscopy before ToF-SIMS analysis. The fluorescence microscopy image of the same area analyzed with ToF-SIMS shows the same spot-like features and a closely matching spatial distribution (Figure 1E), demonstrating that the liposomes can be detected with both methods, and that they produce essentially equal liposome distributions. However, small differences can be observed, primarily as some structures in the ToF-SIMS image are not as evident in the fluorescence image, highlighting the fact that ToF-SIMS only probes the outermost 1−10 nm of the sample surface, and will thus be sensitive to small structures present on the tissue surface, whereas fluorescence microscopy detects all liposomes in the entire tissue section, leading to "amplification" of structures that penetrate the depth of the tissue section.

To verify that the liposomes bind specifically to 6E10 antibodies attached to amyloid-β, an adjacent tissue section was prepared using an identical protocol but without incubation with 6E10 antibodies and neutravidin, as control sample. ToF-SIMS analysis of the control sample in the same area visualized

dx.doi.org/10.1021/ja5019145 | J. Am. Chem. Soc. 2014, 136, 9973−9981

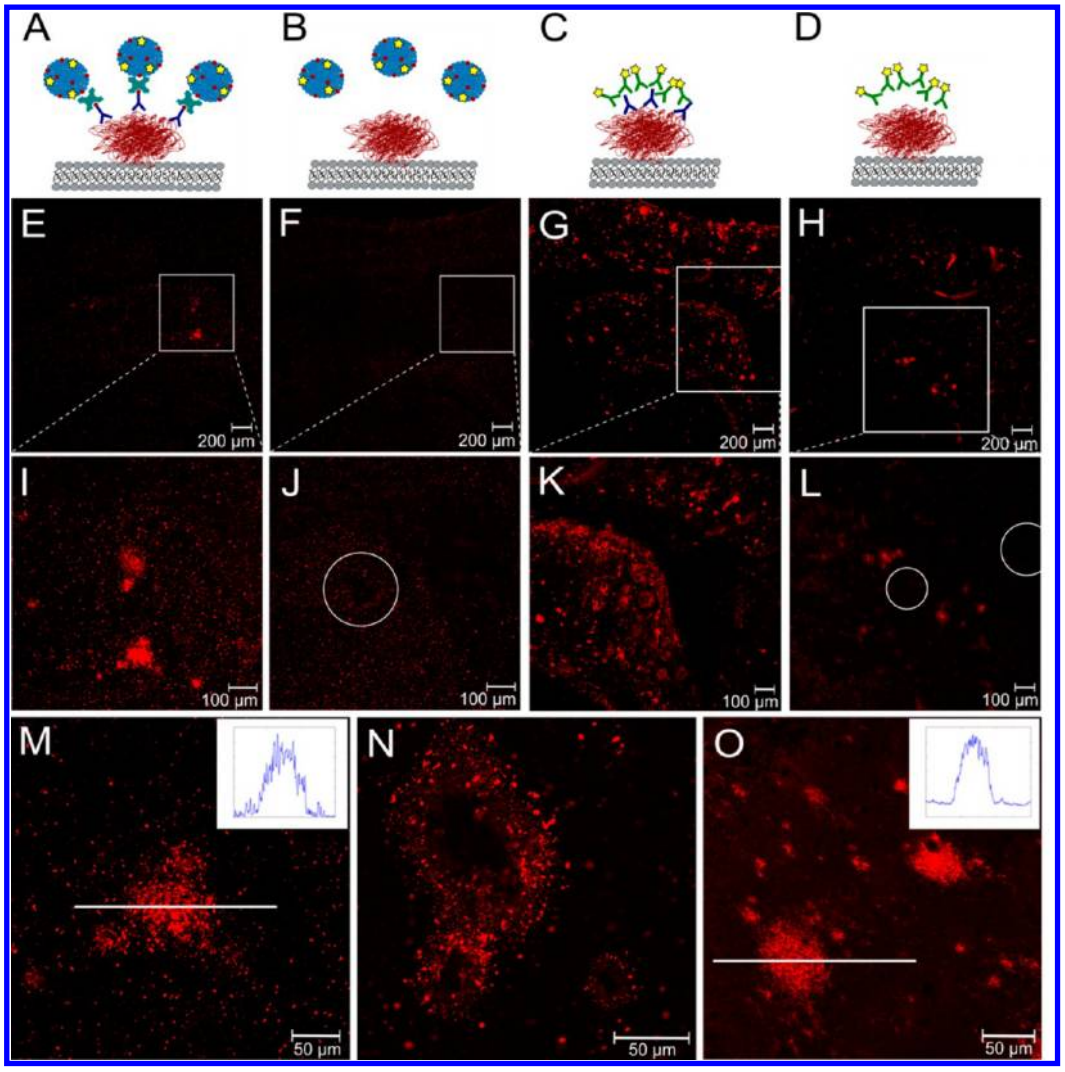

Figure 2. Binding of liposomes and secondary antibodies to 6E10-labeled amyloid-β in transgenic Tg2576 AD mouse brain tissue visualized by fluorescence confocal microscopy. (A,E,I,M,N) Specific binding of liposomes to amyloid-β via biotinylated 6E10 antibodies and neutravidin, (B,F,J) unspecific binding of liposomes to the tissue section (without 6E10 or neutravidin), (C,G,K,O) specific binding of secondary antibodies to amyloid-β via the primary antibody 6E10, and (D,H,L) unspecific binding of secondary antibodies (without 6E10). Fluorescence images were recorded at 5× (E–H), 10× (I–L), 25× (M,O) and 40× (N) magnification. The squares delineated in (E–H) indicate the areas magnified in (I–L). The white circles in (J) and (L) indicate the location of amyloid-β deposits, as observed by bright field microscopy. The insets in (M) and (O) show line profiles of the fluorescence signal across a single deposit (indicated by the lines).

in Figure 1C showed no significant D13-POPC signal, despite the presence of abundant amyloid-β deposits (observed by optical microscopy), indicating negligible unspecific binding of liposomes to amyloid-β deposits (Figure 1D). As another control, a tissue sample from an age-matched wild-type mouse brain was investigated using the same preparation protocol, including incubation with 6E10, neutravidin and biotinylated liposomes. ToF-SIMS analysis of this sample showed only very low unspecific binding of liposomes to the tissue surface (Figure S2 in Supporting Information).

Validation of Antibody-Coupled Liposomes for Detection of Amyloid-β Deposits. To validate the binding of antibody-coupled liposomes to amyloid-β in the tissue samples, conventional immunohistochemical staining and fluorescence microscopy[17] were used to compare the liposome binding with the binding of fluorescent secondary antibodies to amyloid-β via 6E10 as the primary antibody. A schematic illustration of the different approaches is shown in Figure 2A–D. Using liposome binding (Figure 2A,E,I), several amyloid-β deposits were detected, whereas the control sample (without preincubating the tissue with 6E10 and neutravidin) displayed very low amounts of unspecific binding in the same area (Figure 2B,F,J). Using secondary antibodies to detect amyloid-β deposits in the tissue (Figure 2C,G,K), similar but more abundant structures were observed in the fluorescence microscopy images, as compared to the corresponding liposome binding case. Although analysis of a control sample, without incubation with 6E10 primary antibodies, revealed significant binding of secondary antibodies to the tissue surface (Figure 2D,H,L), this unspecific binding cannot entirely explain the greater amount of binding of secondary antibodies to 6E10 per se, as compared to the liposomes. Furthermore, only the most prominent secondary antibody structures (Figure 2G,K) could be correlated to amyloid-β deposits in images obtained by bright field microscopy, suggesting that the higher amount of secondary antibody binding is mainly due to more efficient binding to small amyloid-β structures (which are not visible in the bright field images).

dx.doi.org/10.1021/ja5019145 | J. Am. Chem. Soc. 2014, 136, 9973–9981

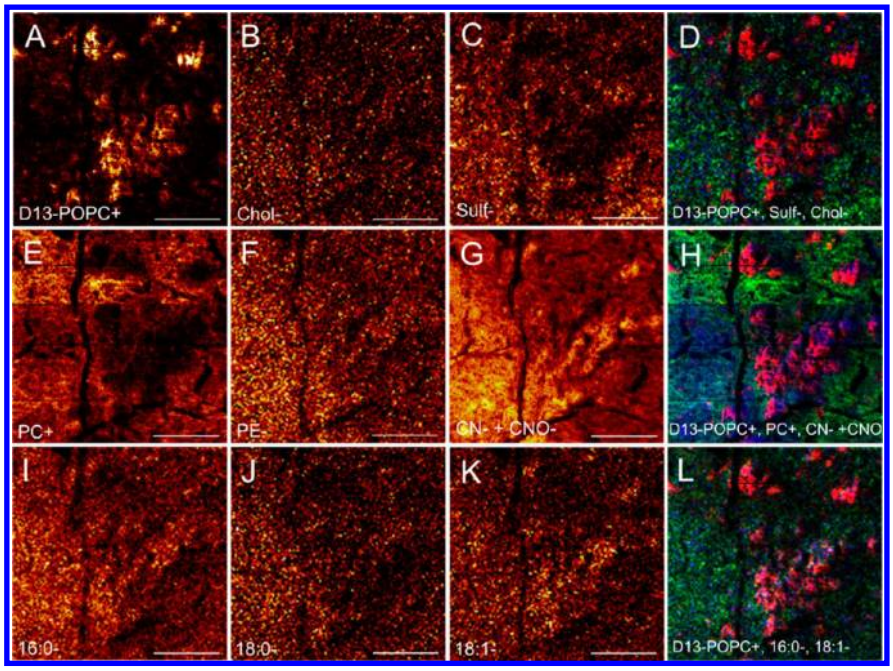

Figure 3. High resolution ToF-SIMS images of liposomes bound to 6E10-labeled amyloid-β deposits and selected lipids in transgenic AD mouse brain tissue. (A) D13-POPC (liposomes), (B) cholesterol ($Chol^-$), (C) sulfatides (Sulf), (D) overlay showing liposomes (red), sulfatides (green) and cholesterol (blue), (E) phosphatidylcholine (PC), (F) phosphatidyletanolamine (PE), (G) CN^- and CNO^- ions, (H) overlay showing liposomes (red), PC (green) and CN^- + CNO^- (blue), (I) palmitic acid (16:0), (J) stearic acid (18:0), (K) oleic acid (18:1), (L) overlay showing liposomes (red), palmitic acid (green) and oleic acid (blue). See Table S1 in Supporting Information for mass peaks used to produce the ToF-SIMS images. Purple color in the overlays indicate colocalization of red and blue in the image, and cyan color represents colocalization of green and blue. Scale bar = 50 μm.

Although the results clearly show that both liposomes and secondary antibodies bind specifically to amyloid-β in the tissue sample (via 6E10/neutravidin and 6E10, respectively), significant differences in the binding can be observed at higher magnifications (Figures 2M−O). Using liposomes to stain the 6E10-labeled deposits produces a "spot-like" distribution, while the secondary antibody binding results in a more homogeneous distribution across the deposits. This difference in binding between liposomes and secondary antibodies is further illustrated by the line profiles presented in Figure 2M,O, which show the fluorescence signal intensity across single deposits (indicated by the white line). Whereas the absolute fluorescence signal along the line profile is similar between the two cases (same settings and intensity scales in the two line profiles), the liposomes produce considerably larger intensity variations as a result of the "spot-like" fluorescence distribution pattern, but also a significantly lower background (outside the deposit), as compared to the secondary antibody case. The larger signal variation associated with the liposome approach, as well as the more abundant structures observed using secondary antibodies, indicate less efficient binding of liposomes compared to secondary antibodies, possibly due to limited accessibility of the liposomes, and may point to further needs for optimization of the liposome incubation protocol. However, the limitation in liposome binding will most likely be less critical for the ToF-SIMS measurements, since ToF-SIMS only probes the outermost surface of the tissue sample, where the liposome access can be expected to be high.

The liposome approach used to stain amyloid-β deposits resulted in two different binding patterns observed in the fluorescence microscopy images: (1) staining of the entire deposit including the core (Figure 2M) or (2) staining of the outer region of the deposit only (Figure 2N). The latter case was not observed when using secondary antibodies to stain the amyloid-β deposits, indicating that secondary antibodies stain the entire deposit, whereas liposomes may not under certain conditions be able to bind to 6E10 at inner regions of the deposits.

Simultaneous Imaging of Amyloid-β and Lipids. An important aspect of the proposed liposome approach is the possibility to simultaneously image the distribution of lipids and peptides/proteins in the tissue. In addition, since the information depth of the ToF-SIMS detection is very shallow (1−10 nm), this approach provides a reliable way to colocalize proteins and lipids at the outermost surface of the tissue. Figure 3 presents ToF-SIMS images of antibody-coupled liposomes and selected lipids in a tissue area containing amyloid-β deposits. The liposome ion image (D13-POPC, Figure 3A) shows a strongly inhomogeneous particle-like distribution, consistent with staining of amyloid-β deposits. In contrast, the phosphatidylcholine (PC) ion image (Figure 3E) displays low signal in areas with high liposome signal but a relatively homogeneous distribution elsewhere, indicating reduced concentration of PC in the amyloid-β deposits and/or extensive liposome binding on top of the amyloid-β deposits, which may shield the PC signal. Analysis of a model system showed that a full liposome layer shields the signal from an underlying PEG layer on the substrate surface to ~20% of its value without the liposomes (see Figure S3 in Supporting Information). However, another phospholipid, phosphatidylethanolamine (PE, Figure 3F), is more homogeneously distributed in the analysis area, even at the liposome-binding sites, contradicting the interpretation that the liposomes are shielding lipid signals at the amyloid-β binding sites. Sulfatides, in general, (Figure

dx.doi.org/10.1021/ja5019145 | J. Am. Chem. Soc. 2014, 136, 9973−9981

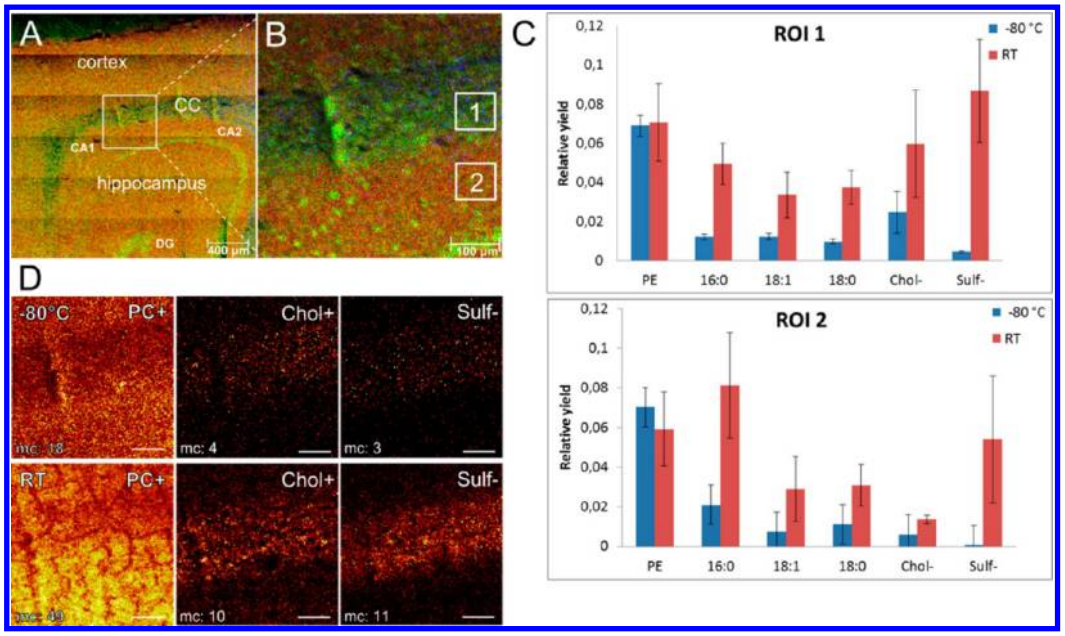

Figure 4. Comparison of ToF-SIMS data obtained from untreated, frozen tissue (at −80 °C) and after antibody/liposome incubation. (A,B) ToF-SIMS images showing the position of the analysis area (white square in (A)) and regions of interest (ROI) (square 1 and 2 in (B)) from which ToF-SIMS data was acquired for comparison of the two different conditions. Overlay of PO_2^- (red), CN^- + CNO^- (green) and cholesterol$^-$ (blue) ions. CC = corpus callosum, DG = dentate gyrus, CA1, CA2 refer to the different areas of the Cornu Ammonis. Field of view: (A) 2.4 × 2.4 mm^2 and (B) 500 × 500 μm^2. (C) Comparison of signal intensities (normalized to the added signal from CH^- and C_2H^-) from selected lipid ions obtained from ROI 1 and 2, respectively, at the two different tissue conditions (untreated, analyzed at −80 °C (blue) and after liposome incubation, analyzed at room temperature (RT, red)). For lipid abbreviation see Table S1 in Supporting Information. The error bars represent the standard deviation of three different tissue samples (n = 3). (D) ToF-SIMS images of the same region as in (B) acquired from an untreated tissue sample (−80 °C, upper row) and after liposome incubation (RT, lower row) displaying the distributions of selected lipids in an area including corpus callosum. mc = maximum counts in one pixel. Scale bar = 100 μm.

3C) are mainly complementarily distributed around the deposits but do also, interestingly, show slightly enhanced signal intensity adjacent to some of the deposits (pseudocolored green in Figure 3D). Cholesterol (Figure 3B) shows a similar distribution pattern as sulfatides, but is more homogeneously distributed across the analysis area. One of the fatty acids, stearic acid (Figure 3J), is mainly homogeneously distributed over the analysis area, whereas oleic and palmitic acid partially colocalize with the liposomes (Figure 3I,K). Since oleic and palmitic acid are fatty acid components of D13-POPC in the liposomes, enhanced signal intensity of these peaks is expected, and represents an artifact arising from the preparatory procedure. Nevertheless, slightly enhanced signal in regions adjacent to the deposits can also be observed (pseudocolored green and blue in Figure 3L). Similarly, the ion signal corresponding to unspecific protein and peptide fragments (CN^- + CNO^-) was also found to partially colocalize with the liposomes (Figure 3G), which may be explained by the peptide content in the amyloid-β deposits or by the presence of neutravidin and/or 6E10 antibodies on top of the amyloid-β deposits.

Effect of Sample Preparation on Lipid Distributions. Handling and preparation of biological tissue might alter the chemical composition and spatial distribution of analytes on the tissue surface.[26−28] In immunohistochemistry, chemical fixatives such as paraformaldehyde (PFA) are normally used to preserve the morphology of the tissue via protein cross-linking reactions. However, the spatial distribution of lipids and other analytes may be affected and chemical structures may be modified by this type of treatment. In order to investigate such effects of the preparation protocol used in this work, the tissue lipid distribution was monitored both before (untreated, frozen tissue analyzed at −80 °C) and after the entire tissue preparation protocol, including PFA fixation and antibody/liposome incubation. For this purpose, an easily recognizable brain region was selected and analyzed in several samples at both conditions (see Figure 4A,B). Spectra were compared for regions of interest (ROI's) selected from a white matter area in corpus callosum and a gray matter area in hippocampus, respectively. The relative ion yield of selected lipids, normalized to the sum of the reference peaks CH^- and C_2H^-, is presented in Figure 4C for each ROI. Notably, almost all lipid ion signals were enhanced after the tissue preparation, including cholesterol, sulfatides and fatty acids, such as palmitic (16:0), oleic (18:1) and stearic acid (18:0). This lipid signal enhancement is most likely caused by changes in the chemical environment (matrix effects) due to rinsing and removal of salts from the surface,[33,34] but it could also depend, completely or partly, on migration of lipids from deeper layers of the tissue onto the surface.[26,33,35] An exception from the general signal enhancement was phosphatidylethanolamine (PE), which displayed no significant change after the preparation. A likely explanation for this lack of signal enhancement is that the primary amine of the PE headgroup may undergo cross-linking reactions with PFA and that this reaction will reduce the yield of the probed PE headgroup ions.

Figure 4D compares the lateral distribution of different lipids in corpus callosum and hippocampus (same region as Figure 4B) before (at −80 °C) and after (at room temperature, RT) preparing the sample with the liposome incubation protocol. In the corresponding mass spectra, shown in Figure S1 in Supporting Information, the increased signal intensities of

dx.doi.org/10.1021/ja5019145 | J. Am. Chem. Soc. 2014, 136, 9973−9981

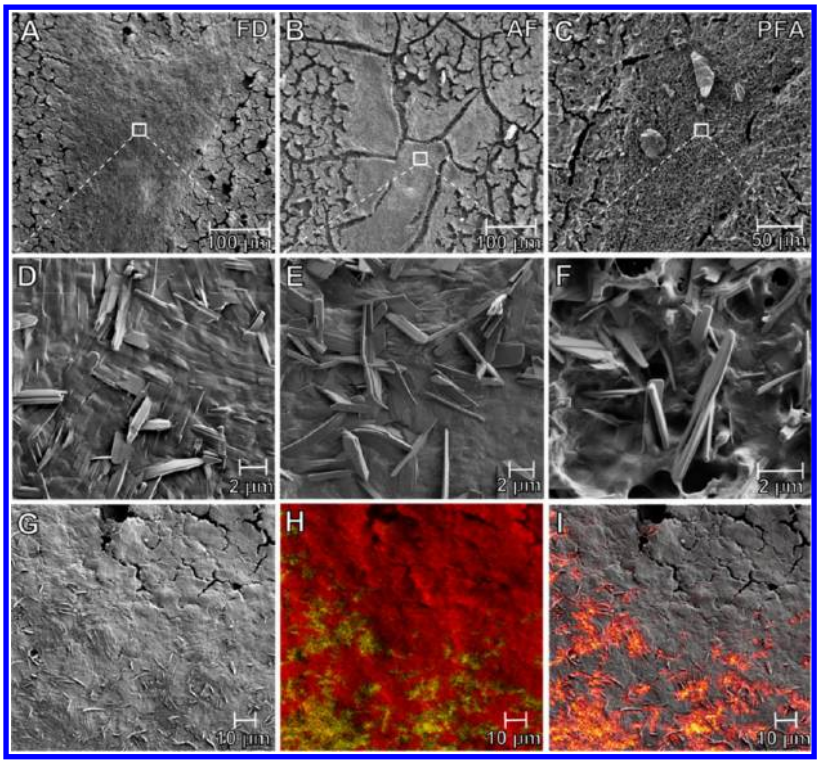

Figure 5. SEM images recorded in an area including arbor vitae in cerebellum after different preparation steps: (A) freeze-dried (FD), (B) rinsed in ammonium formate (AF) followed by plunge-freezing and freeze-drying, (C) fixed with paraformaldehyde (PFA) and rinsed in AF followed by plunge-freezing and freeze-drying. (D–F) Magnified images from the white matter regions indicated by squares in (A–C). (G) SEM image from the border between white (arbor vitae) and gray (granular cell layer) matter in cerebellum. (H) ToF-SIMS positive ion image (high lateral resolution) of the same analysis area as in (G), showing the total ion distribution in red and cholesterol ions in green (the yellow color is produced by overlapping red and green). (I) Superimposed SEM (gray) and cholesterol ToF-SIMS images (red/orange) from G and H.

several lipids, such as phospholipids, cholesterol, fatty acids and sulfatides are clearly visible. Furthermore, no additional peaks were observed in the spectra as a result of the liposome incubation protocol, except for the added deuterated liposomes (D13-POPC). Despite the observed signal increase for some lipids, their lateral distributions were not significantly altered after the preparation, showing some lipids specifically localized to the white matter of corpus callosum (such as cholesterol and sulfatides) and others to the gray matter (such as phosphatidylcholine). It should be noted, however, that these images were recorded at high mass resolution (spatial resolution 3–4 μm) over relatively large analysis areas (500 × 500 μm^2) and changes in the spatial distributions at smaller length scales may still occur.

Effect of Sample Preparation on Tissue Surface Morphology. In order to further investigate the effects caused by the liposome incubation protocol, the tissue surface morphology was analyzed by scanning electron microscopy (SEM). A region including arbor vitae of cerebellum, a structure containing white matter, was analyzed after different steps of the preparation protocol, namely, (1) after freeze-drying (no rinsing or fixation), (2) after rinsing in ammonium formate (AF), followed by plunge-freezing and freeze-drying, and (3) after fixation with PFA, rinsing in AF, plunge-freezing and freeze-drying. Significant differences in surface morphology were observed between the different preparation steps (Figure 5). After rinsing the tissue sample with AF followed by plunge-freezing and freeze-drying, several large tissue fractures extending through the white matter region were observed (Figure 5B), which were not present in the tissue sample that had not been subjected to rinsing (Figure 5A). Chemical fixation with PFA resulted in formation of a small porous structure at the tissue surface (Figure 5C,F). However, the large fractures observed in the AF-rinsed tissue (Figure 5B) were significantly fewer and smaller in the PFA-fixed tissue, suggesting better tissue preservation.

Higher magnification images (Figure 5D,E,F) revealed the presence of abundant elongated particles in the white matter region. These particles were equally shaped and abundant after each of the investigated preparation steps. Furthermore, comparing a SEM image (Figure 5G) with ToF-SIMS images recorded from the same analysis area (Figure 5H), cholesterol was found to be localized in close proximity of, but not overlapping with, the elongated particles (Figure 5I). This observation suggests that the particles, given their elongated shape and their localization in the white matter, may represent fragments of the myelin sheath (which primarily consist of cholesterol).

■ CONCLUSIONS

In this work, a novel analytical approach for simultaneous imaging of lipids and proteins in tissue samples is presented. The approach relies on the use of antibodies to specifically link liposomes to proteins on the tissue surface and subsequently image the spatial distribution of the liposomes with ToF-SIMS. By using deuterated lipids, the liposomes can be distinguished from endogenous lipids, thus allowing for simultaneous visualization of proteins, lipids and other analytes in the tissue. The method was used to visualize the distribution of amyloid-β deposits and a variety of lipids in brain tissue from a transgenic

dx.doi.org/10.1021/ja5019145 | J. Am. Chem. Soc. 2014, 136, 9973–9981

mouse model of AD, and the results obtained by imaging ToF-SIMS were verified using confocal fluorescence immunohistochemistry. Compared to frozen untreated samples, the liposome-binding preparation protocol was found to generate enhanced signal intensities from most lipids, but otherwise not severely affect the tissue integrity and the spatial lipid distributions (at the ≥3−4 μm scale). Importantly, since liposomes can bind to neutravidin coupled to any biotinylated antibody, this technique allows for imaging ToF-SIMS analysis of any peptide or protein of interest in the tissue sample. Furthermore, whereas only one peptide was included in the present study, the method can be used to simultaneously target several different peptides or proteins, by coupling different antibodies to liposomes made of different "fingerprint" lipids. The possibility to simultaneously image proteins, lipids and other biomolecules, which in principle is possible with the imaging ToF-SIMS methodology presented here, offers new opportunities to study molecular interactions in complex biological samples such as brain tissue and may therefore contribute to an increased understanding of the pathogenesis of different neurodegenerative diseases, such as AD.

■ ASSOCIATED CONTENT

Supporting Information

Table of the mass spectrum peaks used in the presented ToF-SIMS results, including their ion assignments, positive and negative spectra of a mouse brain tissue sample recorded before and after liposome incubation, ToF-SIMS images of a wild-type mouse brain and a diagram showing the substrate ToF-SIMS signal upon liposome binding to a model surface. This material is available free of charge via the Internet at http://pubs.acs.org.

■ AUTHOR INFORMATION

Corresponding Author

peter.sjovall@sp.se

Present Addresses

[#]Anders Gunnarsson, Discovery Science, AstraZeneca R&D, S-43183 Mölndal, Sweden.

[▽]Santiago Solé-Domènech, (1) Department of Biochemistry, Weill Cornell Medical College, Box 63, 1300 York Ave, New York, NY 10065, (2) Department of Experimental Medical Science, Experimental Dementia Research Unit, Wallenberg Neuroscience Center, Lund University, 221 84 Lund, Sweden.

Author Contributions

The manuscript was written through contributions of all authors. All authors have given approval to the final version of the manuscript.

Notes

The authors declare no competing financial interest.

■ ACKNOWLEDGMENTS

The authors would like to thank Prof. Thomas Hökfelt for useful advice in the beginning of the project. This project was funded by the Swedish Research Council (VR), the Swedish Governmental Agency for Innovations Systems (VINNOVA), the Wallenius Foundation and the EMRP projects IND15 "SurfChem" and HLT04 "BioSurf". The EMRP is jointly funded by the EMRP participating countries within EURAMET and the European Union.

■ REFERENCES

(1) Wenk, M. R. *Nat. Rev. Drug Discovery* **2005**, *4*, 594.
(2) Di Paolo, G.; Kim, T. W. *Nat. Rev. Neurosci.* **2011**, *12*, 284.
(3) Hur, J.-Y.; Welander, H.; Behbahani, H.; Aoki, M.; Frånberg, J.; Winblad, B.; Frykman, S.; Tjernberg, L. O. *FEBS J.* **2008**, *275*, 1174.
(4) Beel, A. J.; Sakakura, M.; Barrett, P. J.; Sanders, C. R. *Biochim. Biophys. Acta, Mol. Cell Biol. Lipids* **2010**, *1801*, 975.
(5) St George-Hyslop, P. H. *Sci. Am.* **2000**, *283*, 76.
(6) Puglielli, L.; Tanzi, R. E.; Kovacs, D. M. *Nat. Neurosci.* **2003**, *6*, 345.
(7) Ehehalt, R. *J. Cell Biol.* **2003**, *160*, 113.
(8) Han, X. L. *Biochim. Biophys. Acta, Mol. Cell Biol. Lipids* **2010**, *1801*, 774.
(9) Touboul, D.; Laprevote, O.; Brunelle, A. *Curr. Opin Chem. Biol.* **2011**, *15*, 725.
(10) Pol, J.; Strohalm, M.; Havlicek, V.; Volny, M. *Histochem. Cell Biol.* **2010**, *134*, 423.
(11) Benabdellah, F.; Seyer, A.; Quinton, L.; Touboul, D.; Brunelle, A.; Laprévote, O. *Anal. Bioanal. Chem.* **2010**, *396*, 151.
(12) Rohner, T. C.; Staab, D.; Stoeckli, M. *Mech. Ageing Dev.* **2005**, *126*, 177.
(13) Touboul, D.; Halgand, F.; Brunelle, A.; Kersting, R.; Tallarek, E.; Hagenhoff, B.; Laprevote, O. *Anal. Chem.* **2004**, *76*, 1550.
(14) Sjövall, P.; Lausmaa, J.; Johansson, B. *Anal. Chem.* **2004**, *76*, 4271.
(15) Nygren, H.; Borner, K.; Hagenhoff, B.; Malmberg, P.; Mansson, J. E. *Biochim. Biophys. Acta* **2005**, *1737*, 102.
(16) Tahallah, N.; Brunelle, A.; De La Porte, S.; Laprevote, O. *J. Lipid Res.* **2008**, *49*, 438.
(17) Solé-Domènech, S.; Sjövall, P.; Vukojevic, V.; Fernando, R.; Codita, A.; Salve, S.; Bogdanovic, N.; Mohammed, A. H.; Hammarström, P.; Nilsson, K. P. R.; LaFerla, F. M.; Jacob, S.; Bergren, P.; Giménez-Llort, L.; Schalling, M.; Terenius, L.; Johansson, B. *Acta Neuropathol.* **2013**, *125*, 145.
(18) Lazar, A.; Bich, C.; Panchal, M.; Desbenoit, N.; Petit, V. W.; Touboul, D.; Dauphinot, L.; Marquer, C.; Laprévote, O.; Brunelle, A.; Duyckaerts, C. *Acta Neuropathol.* **2013**, *125*, 133.
(19) Garrison, B. J.; Postawa, Z. *Mass Spectrom. Rev.* **2008**, *27*, 289.
(20) Bich, C.; Vianello, S.; Guerineau, V.; Touboul, D.; De La Porte, S.; Brunelle, A. *Surf. Interface Anal.* **2013**, *45*, 260.
(21) Guerquin-Kern, J.; Wu, T.; Quintana, C.; Croisy, A. *Biochim. Biophys. Acta* **2005**, *1724*, 228.
(22) Senyo, S. E.; Steinhauser, M. L.; Pizzimenti, C. L.; Yang, V. K.; Cai, L.; Wang, M.; Wu, T.-D.; Guerquin-Kern, J.-L.; Lechene, C. P.; Lee, R. T. *Nature* **2013**, *493*, 433.
(23) Wilson, R. L.; Frisz, J. F.; Hanafin, W. P.; Carpenter, K. J.; Hutcheon, I. D.; Weber, P. K.; Kraft, M. L. *Bioconjugate Chem.* **2012**, *23*, 450.
(24) Kraft, M. L.; Weber, P. K.; Longo, M. L.; Hutcheon, I. D.; Boxer, S. G. *Science* **2006**, *313*, 1948.
(25) Gunnarsson, A.; Sjövall, P.; Höök, F. *Nano Lett.* **2010**, *10*, 732.
(26) Sjövall, P.; Johansson, B.; Lausmaa, J. *Appl. Surf. Sci.* **2006**, *252*, 6966.
(27) Malm, J.; Giannaras, D.; Riehle, M. O.; Gadegaard, N.; Sjövall, P. *Anal. Chem.* **2009**, *81*, 7197.
(28) Belazi, D.; Solé-Domènech, S.; Johansson, B.; Schalling, M.; Sjövall, P. *Histochem. Cell Biol.* **2009**, *132*, 105.
(29) Hsiao, K.; Chapman, P.; Nilsen, S.; Eckman, C.; Harigaya, Y.; Younkin, S.; Yang, F.; Cole, G. *Science* **1996**, *274*, 99.
(30) Mayer, L. D.; Hope, M. J.; Cullis, P. R. *Biochim. Biophys. Acta, Biomembr.* **1986**, *858*, 161.
(31) Jousma, H.; Talsma, H.; Spies, F.; Joosten, J. G. H.; Junginger, H. E.; Crommelin, D. J. A. *Int. J. Pharm.* **1987**, *35*, 263.
(32) Sjövall, P.; Rading, D.; Ray, S.; Yang, L.; Shard, A. G. *J. Phys. Chem. B* **2009**, *114*, 769.
(33) Jones, E. A.; Lockyer, N. P.; Vickerman, J. C. *Anal. Chem.* **2008**, *80*, 2125.
(34) Robinson, M.; Castner, D. *Biointerphases* **2013**, *8*, 15.
(35) Bich, C.; Havelund, R.; Moellers, R.; Touboul, D.; Kollmer, F.; Niehuis, E.; Gilmore, I. S.; Brunelle, A. *Anal. Chem.* **2013**, *85*, 7745.